DOI: 10.1021/ma9000429

Macromolecules
ARTICLE

Mesoscopic Simulation of Entangled Polymer Brushes under Shear: Compression and Rheological Properties

Florent Goujon,*,† Patrice Malfreyt,† and Dominic J. Tildesley‡

†*Laboratoire de Thermodynamique et Interactions Moléculaires FRE CNRS 3099, Université Blaise Pascal, 63177 Aubière Cedex, France, and* ‡*Unilever Research Port Sunlight, Bebington, Wirral CH63 3JW, U.K.*

Received January 9, 2009; Revised Manuscript Received May 5, 2009

ABSTRACT: We report a study of the influence of chain entanglements in dissipative particle dynamics simulations of polymer brushes under shear. We observe that the incorporation of an entanglement potential to prevent bond crossings significantly changes the friction and viscosity of these systems. Simulations have been carried out for different compression ratios at constant chemical potential. We have also studied the influence of the solvent quality and the intensity of the shear rate on the thermodynamic, structural, and rheological properties of the system. We show that the behavior of the model polymers is in good agreement with SFA experiments and theoretical scaling laws. The use of an entanglement potential avoids the artificial overlap between polymer particles that often occurs on the mesoscopic scale. We conclude that such a model is necessary for the correct description of the polymer brush system, especially for the calculation of rheological and frictional properties.

Introduction

The coating of a surface with end-grafted polymer chains is an interesting way of changing the mechanical properties of the surface. If the grafting density is high enough, then the chains are oriented normal to the surface, forming a polymer brush. Two sliding solid surfaces can have their friction reduced by three orders of magnitude when coated with such polymer chains.[1] This mechanical effect is not the only application of polymer brushes: they can be used for surface protection, colloidal stabilization,[2−4] surface modification,[5] or biocompatibility. All of these applications require a detailed understanding of the structural and rheological properties of the brush system.

The polymer brushes have been widely studied by theoretical methods.[6−10] Scaling laws have been deduced, describing the scaling behavior of these systems. These systems have been extensively studied using surface force apparatus (SFA) experiments.[1,11−16] Improvements in these techniques have made it possible to measure precisely the normal and tangential components of the pressure when sliding the two surfaces under compression. These experiments are of great importance in understanding the lubrication process.

The polymer brushes system has also been widely studied using various simulation methods. Molecular dynamics has been used to study both the brush structure[17,18] and polymer melts to characterize the entanglement regime.[19,20] However, the time and length scales involved in polymer dynamics are too large to be studied with an all-atom, molecular description. Simulations on the mesoscopic scale are an interesting alternative to model polymer brushes, and stochastic dynamics methods have been successfully applied.[21−28] These methods are specifically designed to model polymer systems far from equilibrium, which is the case when applying a high shear rate. Lattice Monte Carlo methods have also been used to model the mesoscopic scale.[29,30]

*Corresponding author. E-mail: florent.goujon@univ-bpclermont.fr.

Dissipative particle dynamics (DPD) is a coarse-grain method first introduced by Hoogerbrugge and Koelmann.[31,32] As for any mesoscopic method, one DPD particle represents an entire region of the fluid phase. Consequently, the simulated time and length scales are much greater than those in conventional molecular dynamics. Polymer brushes systems have been studied using this method and compared with molecular dynamics.[33] We have shown in previous works that DPD is a useful tool for studying the structural, thermodynamical and rheological properties of polymer brushes.[34−36]

The lubrication effect of the solvent has been shown to be an important factor in those models, so the solvent particles are described explicitly in the model. Many stochastic methods do not generally use a discrete description of the solvent interacting with the polymer brushes. We have shown in a previous paper that the use of a continuum description of the solvent leads to a different description of the rheological properties,[37] particularly during a compression. However, care has to be taken when considering the behavior of soft DPD-like particles because this can result in unphysical overlap. This is a major issue for simulating confined polymers, where the behavior can be strongly governed by the topology. We have recently suggested a bond repulsion potential[38,39] to model polymer brush systems. We have shown that an additional repulsion force between interacting polymer segments prevents the chains from crossing each other, preserving the systems topology.

This work aims to model the compression of polymer brushes using this entanglement DPD model. Using a previously well-established methodology, we plan to study the influence of the entanglement potential on the structural and rheological properties of the system. This article is organized as follows. In the first section, we detail the model used in our simulations. The calculation of the thermodynamical, structural, and rheological properties is outlined, and the different mesoscopic simulation methods are described. The second section contains our results, divided into three parts: The first part details the methodology of simulating a compression and highlights the differences in an entangled and a nonentangled brush system. The scaling

 Published on Web 05/21/2009

behavior of the brushes is compared with theoretical scaling laws and experimental results. The second part deals with the influence of the solvent quality and the shear rate on friction. The third part explains the details in simulation, including the checks of the thermodynamic consistency and the calculation of the rheological properties.

Simulation Model

Dissipative Particle Dynamics Model. Dissipative particle dynamics uses a classical time integration of the forces acting on each particle. We used a modified velocity Verlet algorithm, which gives accurate convergence and is widely used in DPD simulations. The total force acting between two DPD particles, i and j, separated by a distance, r_{ij}, can be split into three pairwise additive contributions. The conservative force, $\mathbf{f}_{ij}^{C}$, derives from a soft repulsion potential and is expressed as

$$\mathbf{f}_{ij}^{C} = \begin{cases} a_{ij}\left(1-\frac{r_{ij}}{r_c}\right)\hat{\mathbf{r}}_{ij} & (r_{ij} < r_c) \\ 0 & (r_{ij} \geq r_c) \end{cases} \quad (1)$$

where a_{ij} is the maximum repulsion parameter, r_c is the cutoff radius, and $\hat{\mathbf{r}}_{ij}$ is the unit vector along the $i-j$ direction. The dissipative force, $\mathbf{f}_{ij}^{D}$, includes the energy loss due to the local friction between the particles. The function of the random force, $\mathbf{f}_{ij}^{R}$, is to input energy to the system to model the Brownian motion, which is of importance for particles interacting on this scale

$$\mathbf{f}_{ij}^{D} = -\gamma\omega^{D}(\hat{\mathbf{r}}_{ij}\cdot\mathbf{v}_{ij})\hat{\mathbf{r}}_{ij} \quad (2)$$

$$\mathbf{f}_{ij}^{R} = \sigma\omega^{R}\theta_{ij}\frac{1}{\sqrt{\delta t}}\hat{\mathbf{r}}_{ij} \quad (3)$$

where σ and γ are constants, ω^{D} and ω^{R} are dimensionless weighting functions, δt is the unit time step, and θ_{ij} is a random number with Gaussian distribution, zero mean, and unit variance. The DPD method has been shown to sample the canonical ensemble if the following relations are satisfied, which follow from the fluctuation−dissipation theorem

$$\gamma = \frac{\sigma^2}{2k_B T} \quad \text{and} \quad \omega^{D}(r_{ij}) = (\omega^{R}(r_{ij}))^2 \quad (4)$$

where k_B is the Boltzmann constant and T is the imposed temperature. Because no explicit form is imposed for the weighting functions, a simple soft repulsive expression has been chosen that is similar to the expression for the conservative force ($\omega_D = 1 - r_{ij}/r_c$).[47] The DPD method uses virtual mesoscopic particles, so the time and length scales require careful consideration. We return to this issue in the next section.

Reduced Units. At the mesoscopic level, it is difficult to have a precise idea of the scales involved in the simulations. The real size of a DPD polymer particle may vary from one to several dozens of monomers, depending on the interaction potential and the time scale. Many recent papers deal with this issue, trying to connect the microscopic and mesoscopic scales.[42−46] Because this work aims at characterizing only the scaling behaviors of polymer brushes, a simple linear repulsion potential has been used for the conservative force. It has been shown by Groot[47] that any soft potential can give a correct description on the mesoscopic scale.

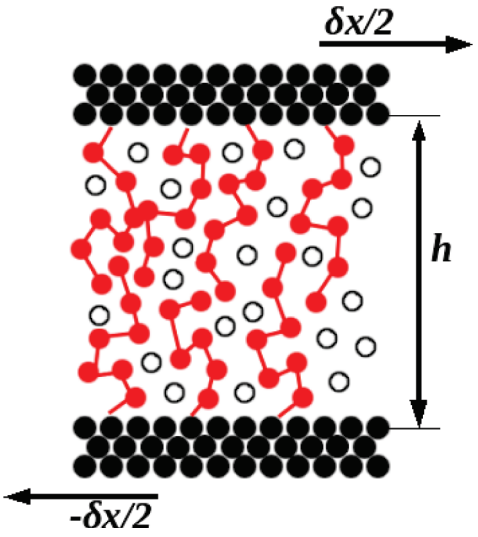

Figure 1. Schematic view of the polymer brushes system. Each solid surface consists of three layers (●) separated by a distance h. Polymer chains are chemically grafted onto each surface and immersed in a good solvent (○). We applied a shear rate by moving the solid surfaces in opposite directions along the x direction.

The unit mass and distance are chosen to be the particle mass, m, and the cutoff radius, r_c. The reduced values are then $m^* = m/m = 1$ and $r^* = r/r_c$. The reduced temperature is expressed using the unit energy, ε, as $T^* = k_B T/\varepsilon = 2.0$. Consequently, the unit of time is $t^* = t(\varepsilon/mr_c^2)^{1/2}$, and the unit interaction parameter is $a^* = a(r_c/\varepsilon)$. Any other unit used in this article can be deduced from these definitions. Because all values calculated in this article are in reduced units, the star notation has been removed for clarity.

The interaction parameter, a_{ij}, is a key value for simulating polymer chains in a solvent of a particular quality. In a previous work, a set of parameters was established[34,35] to model the polymer brushes system efficiently: the reduced interaction parameter is set to $a_{ij} = 60.0$ for any type of particle. Therefore, the polymer−polymer and the solvent−solvent interactions are defined by $a_{pol-pol} = a_{sol-sol} = 60.0$. The value of the polymer−solvent interaction parameter $a_{pol-sol}$ can be set to be equal to, less than, or more than this value to provide an athermal, good, or bad solvent, respectively. In this work, the polymer chains are immersed in a good solvent, defined by $a_{pol-pol} = 40.0$. In a previous paper, we also established the entanglement parameters designed to avoid most bond crossings with a minor influence on the thermodynamic properties of the system. The values $a_{ij}^{ent} = 40.0$ and $r_c^{E} = 0.80$ were found to be optimal.[39]

Polymer Brushes. A polymer chain can be created from DPD particles by adding a simple harmonic spring force between the beads. This simple model has been developed by Schlijper[40,41] and exhibits the behavior of a Gaussian chain. The chains are described in our model by adding a spring force $\mathbf{f}_{ij}^{S}$ acting between two connected particles i and j

$$\mathbf{f}_{ij}^{S} = k_s(r_{ij} - r_{eq})\hat{\mathbf{r}}_{ij} \quad (5)$$

where r_{eq} is the equilibrium bond length and k_s is the spring force constant. The polymer chains are grafted to solid surfaces using the same harmonic force. Figure 1 shows a schematic view of the system: each solid surface consists of three 27 × 20 hexagonal-packed layers tethered to their initial positions by a harmonic force. The z axis is oriented along the normal to the solid surfaces. We applied a shear is applied by moving the surfaces in opposite directions along

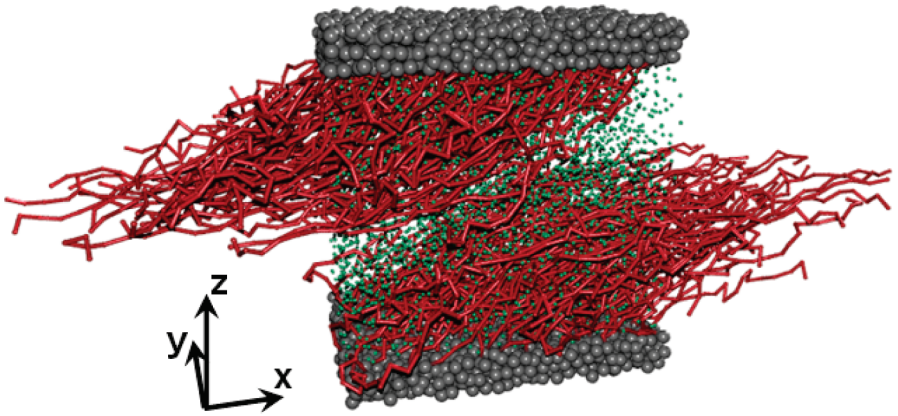

Figure 2. Snapshot of a simulation box containing entangled polymer brushes immersed in solvent at a moderate compression ratio ($h/h_0 = 0.54$). The polymer chains are reconstructed from their grafting point for a better visualization. Different particle sizes are used for clarity. The arrows show the direction of the shear applied to each wall.

the x axis by an amount $x\delta$ in one time step

$$\delta x = \pm\frac{\dot{\gamma}_a L_z}{2}\delta t \tag{6}$$

where $\dot{\gamma}_a$ is the applied shear rate. The reduced time step, δt, is set to 0.01 units of time. A total of 270 polymer chains are grafted onto the two surfaces. Each surface contains 135 randomly grafted chains, which gives an overall grafting density of 0.25. The length of each chain is 20 beads, which gives a total number of 5400 polymer DPD particles. Those chains are immersed in a solvent represented by various numbers of DPD particles, depending on the system size. Figure 2 shows a snapshot of a typical simulation cell under shear.

We have shown in a previous article[39] that this polymer model cannot prevent the bond crossings because of the soft repulsion between the beads. This leads to many violations of the topology of the polymer chains and ignores entanglements. We have included an additional repulsion force between the chain segments to prevent such crossings on the basis of the Kumar and Larson spring−spring repulsion model.[38] The entanglement force, $\mathbf{f}_{ij}^{E}$, is

$$\mathbf{f}_{ij}^{E} = \begin{cases} a_{ij}^{ent}\left(1-\dfrac{d_{ij}}{r_c^{E}}\right)\hat{\mathbf{d}}_{ij} & (d_{ij} < r_c^{E}) \\ 0 & (d_{ij} \geq r_c^{E}) \end{cases} \tag{7}$$

where a_{ij}^{ent} is the maximum repulsion value, $r_c{}^{E}$ is the entanglement cutoff value, and d_{ij} is the minimal distance between the two interacting bond segments i and j. The force is then applied on the polymer beads by using a simple lever rule: each bead receives a fraction of the force corresponding to its distance from the segment interaction point.[38] The calculation of $\mathbf{f}_{ij}^{E}$, the tests for topology violation, and a detailed study of the efficiency of such a model in DPD and polymer brushes can be found in a previous paper.[39]

Thermodynamic and Rheological Properties. The profile of the components of the pressure tensor are calculated using the Irving−Kirkwood definition[48,49]

$$p_{\alpha\beta}(z) = \rho(z)k_B T_{\alpha\beta}(z) - \frac{1}{L_x L_y}\left\langle \sum_i \sum_{j>i} \frac{(r_{ij})_\alpha (\mathbf{f}_{ij})_\beta}{|z_{ij}|}\theta\left(\frac{z-z_i}{z_{ij}}\right)\theta\left(\frac{z_j-z}{z_{ij}}\right)\right\rangle \tag{8}$$

where $< ... >$ denotes a configurational average and α and β represent the x, y, or z directions. The double sum is over all pairs of interacting particles and $\mathbf{f}_{ij}$ is the total force acting between particles i and j. The entanglement contribution is considered to be acting between the two positions calculated on the bonds so that it gives a pairwise contribution, which is easily included in eq 8. The calculation of the local pressure is useful to check the mechanical equilibrium inside the simulation cell because the pressure must be constant through the system. Additionally, the calculation of the tangential pressure component, p_{xz}, allows us to calculate rheological properties. The friction coefficient is defined by the ratio of tangential and normal pressure[50]

$$\varepsilon(z) = -\frac{\langle p_{xz}(z)\rangle}{\langle p_{zz}(z)\rangle} \tag{9}$$

The profile of the shear viscosity, η, of the solvent is

$$\eta(z) = -\frac{\langle p_{xz}(z)\rangle}{\dot{\gamma}(z)} \tag{10}$$

where $\dot{\gamma}(z)$ is the x component of the derivative of the solvent velocity profile with respect to z. The value of η used in this article represents the minimal solvent viscosity value, which corresponds to the middle of the pore.[35]

We also established the chemical equilibrium by calculating the chemical potential of the solvent. To do this, we use the test particle insertion method,[51] calculating the interaction energy of a test particle inserted in the box. Because the local solvent density varies across the simulation cell, we used the definition of the configurational chemical potential first introduced by Widom,[52] which can be used to validate the local chemical equilibrium.[36,53−55]

$$\mu^{conf}(z) = k_B T \ln\left[\frac{\langle\rho(z)\rangle_{NVT}}{\left\langle\exp\left(-\frac{\Delta U^{test}}{k_B T}\right)\right\rangle_{NVT}}\right] = k_B T \ln\langle Z(z)\rangle_{NVT} \tag{11}$$

In this equation, $\rho(z)$ is the solvent number density and ΔU^{test} is the interaction energy of the test particle at height z with the other N particles in the cell. A demonstration of the thermodynamic consistency of the simulation is provided in the last section of the discussion.

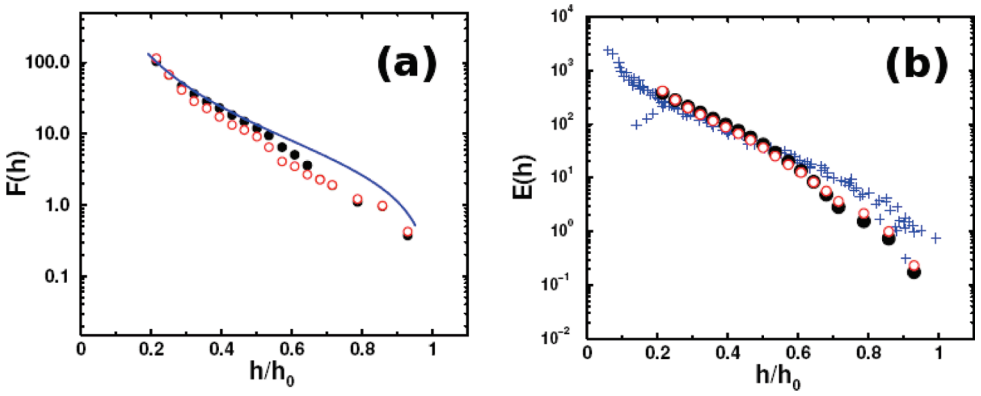

Figure 3. (a) Force per unit surface, F, as a function of the compression ratio, h/h_0, for entangled (filled symbols) and nonentangled (open symbols) polymer brush systems. The values are scaled so that they fit on the same Alexander−de Gennes scaling law (curve). (b) Energy per unit surface, E, as a function of the compression ratio, h/h_0, for entangled and nonentangled systems (● and ○, respectively). The crosses are experimental measurements from SFA by Taunton et al.[61] The values are scaled for comparison.

Grand Canonical Ensemble. We have shown in a previous study that a set of simulations modeling a compression should be conducted at constant chemical potential.[36] Indeed, because we want to simulate various surface separations, the number of solvent particles has to be adjusted. This is done by fixing the chemical potential for the solvent in each simulation. The grand canonical conditions can be readily included in a DPD simulation by performing creation/deletion moves in a dynamical run.[56] We attempt to create or delete a solvent particle with equal probability at given times by using the grand canonical Monte Carlo acceptance rules[57,58]

$$P^{\mathrm{acc}}_{\mathrm{creation}} = \min\left[1, \frac{\langle Z\rangle_z V}{N+1}\exp\left(-\frac{\Delta U}{k_{\mathrm{B}}T}\right)\right] \qquad (12)$$

$$P^{\mathrm{acc}}_{\mathrm{deletion}} = \min\left[1, \frac{N}{\langle Z\rangle_z V}\exp\left(-\frac{\Delta U}{k_{\mathrm{B}}T}\right)\right] \qquad (13)$$

where V is the total cell volume, ΔU is the potential energy of the created/deleted particle interacting with the system, and $Z = \exp(-\mu^{\mathrm{conf}}/k_{\mathrm{B}}T)$ is the activity of the solvent related to the imposed chemical potential. The details of this modified code are described in a previous paper.[36] The velocity of the inserted particle is chosen randomly using a Maxwell−Boltzmann distribution using the imposed temperature. To take into account the shear along the x direction, the x component of the solvent particle velocity is changed by the addition of the x component of the streaming velocity.

Results and Discussions

Compression under Shear. The methodology for simulating a compression in DPD is as follows. A reference system is chosen for which the opposite brushes do not overlap, with the smallest distance between the solid surfaces. This system is equilibrated over 100 000 timesteps. The solvent chemical potential, μ, is then calculated during a 300 000 timestep acquisition at constant NVT and considered to be the reference chemical potential. We then perform other simulations by decreasing the separation, h, between the walls. These simulations are carried at constant μVT. The compression ratio is h/h_0, where h_0 is the surface separation of the reference system. Consequently, low values of the compression ratio correspond to a high compression. Each constant μVT simulation is 500 000 timesteps long, trying a creation/deletion move every 500 timesteps. The number of solvent particles is stabilized after a first run, and the acquisition is done during a second one.

The interpenetration coefficient, I, between the brushes is defined as

$$I = \frac{\int_0^{h/2}\rho_1(z)\,\mathrm{d}z}{\int_{-h/2}^{h/2}\rho_1(z)\,\mathrm{d}z} \qquad (14)$$

where $\rho_1(z)$ is the number density profile of a single brush considering the origin of the z axis at the middle of the cell. The reduced interaction parameter, $a_{\mathrm{pol-sol}}$, is set to 40.0, which is characteristic of a good solvent. The reference separation was found to be $h_0 = 28$. We use a total number density of $\rho = 4$, which corresponds to a dense liquid.[47] This gives a reference chemical potential of $\mu^{\mathrm{conf}} = 36.5$. A total of 18 compression ratios have been simulated, ranging from $h = h_0 = 28$ ($h/h_0 = 1.0$) to $h = 7$ ($h/h_0 = 0.25$). The corresponding number of solvent particles ranges from approximately 12 900 to 50, respectively. A shear rate $\dot{\gamma}_{\mathrm{a}} = 0.10$ is applied for each simulation. Two sets of simulations are run: the first one uses bond repulsions to exclude unphysical polymer crossing (the entangled polymer), the second one is used as a reference without those entanglement forces.

As in previous studies,[36,37] it is important to study the scaling behavior of the polymer brushes system under compression. A model for polymer chains attached to surfaces under good solvent conditions has been proposed by Alexander[59] and further extended by de Gennes.[7,60] The force per unit area, $F(h)$, is defined as the difference between the pressure at a given compression ratio and the pressure of the reference system

$$F(h) = p_{zz}(h) - p_{zz}(h_0) \qquad (15)$$

The Alexander−de Gennes theory for compressed polymer brushes gives the following analytical expression for $F(h)$

$$F(h) \propto \left[\left(\frac{h_0}{h}\right)^{9/4} - \left(\frac{h}{h_0}\right)^{3/4}\right] \qquad (16)$$

The first term of eq 16 comes from the osmotic pressure and is predominant for strong compressions. The second term describes the elastic term of the polymer chains. Figure 3a shows the force−distance profile for the entangled

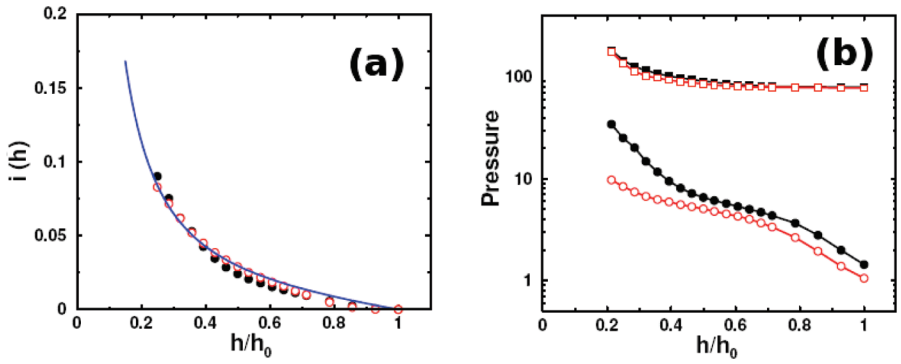

Figure 4. (a) Brush interpenetration coefficient as a function of the compression ratio for entangled (filled symbols) and nonentangled (open symbols) polymer brushes. The values are shifted horizontally to fit the same scaling law (eq 18), represented by the curve. (b) Values of the p_{zz} (square symbols) and p_{xz} (circle symbols) components of the pressure tensor as a function of the compression ratio. Filled and open symbols are used for entangled and nonentangled systems, respectively.

and nonentangled polymer brushes compared with the Alexander−de Gennes theory. The two sets of values from the simulations have been scaled so that they fit eq 16 at high compression. We can see that both systems exhibit a similar scaling behavior, and the Alexander−de Gennes theory is followed. Note that the divergence at low compression comes from the logarithmic scale and the fluctuations of the measured pressures, which are on the same order as $F(h)$ at these compression ratios.

The interaction energy per unit area, can be deduced from $F(h)$ by

$$E(h) = \int_h^{h_0} F(h')\,\mathrm{d}h' \tag{17}$$

$E(h)$ can be accessed experimentally. Figure 3b shows the values of $E(h)$ calculated from the two sets of simulations. Experimental values obtained by SFA[12,61] have been added for comparison. It is interesting to note that the improvement of the DPD model by the addition of bond repulsion does not change the scaling behavior of the system under compression already observed in our previous simulations.[36] However, the main difference between entangled and nonentangled systems has been shown to be in the structure of the brushes:[39] the repulsion is stronger between the polymer chains, which gives rise to a swelling of the brush. As a consequence, we have calculated the interpenetration coefficient, I, to be a function of h/h_0. The Alexander−de Gennes theory suggests that $I(h)$ is

$$I(h) \propto \left(\frac{h}{h_0}\right)^{-4/3}\left[1-\left(\frac{h}{h_0}\right)^3\right] \tag{18}$$

Figure 4a shows the interpenetration coefficient for both sets of simulations. The values of I have been scaled to fit the same scaling law, represented by the continuous line. The scaling behavior of the brush overlap fits with the theoretical predictions for both sets of simulations. We can then see that the addition of entanglement gives the scaling description of the polymer brushes for both structural and thermodynamical properties, as well as for the systems without entanglements. The structure change and the influence of the solvent quality will be studied in more detail in the next section.

We now focus on the rheological properties of the polymer brushes system during the compression under shear. Considering a polymer brush at low compression, the repulsions between chain segments induced by the entanglement forces cause the brushes to extend, which causes an increase in the interpenetration. As the compression ratio decreases, the overlap of the brushes increases, which should intuitively result in an increase in the friction coefficient. Previous studies of the compression under shear show a decrease or a plateau in the friction values as the system is compressed. Figure 4b shows the values of the normal and tangential pressure tensor components (p_{zz} and p_{xz}, respectively) for both sets of simulations.

Considering the nonentangled system, the increase in p_{xz} during the second part of the compression ($0.2 < h/h_0 < 0.5$) is only 93%, whereas p_{zz} increases 107%. This results in a limiting value of the friction, which was previously interpreted as a strong lubricant effect.[37] As we can see in Figure 4b, the behavior of the entangled system is very different because the tangential pressure increases radically at low compression ratio. As a comparison, the increase in p_{zz} is similar to that of the nonentangled system (102%), but the tangential component is increased by 423% in the high compression domain ($0.2 < h/h_0 < 0.5$). This is in agreement with a strong interpenetration between brushes: because this model includes segment repulsions, the shear rate imposes strong interactions between sliding chains of opposite walls.

The effect of the entanglement force can be quantified by the number of topology violations, that is, bond crossings per time step. Using no entanglement force, a system at low compression ($h/h_0 = 20$) contains an average of 1.5 crossings per time step, and the addition of the entanglement force makes this number fall to 0.03 crossings per time step. Those two results increase to 11.3 and 0.7, respectively, for a highly compressed system ($h/h_0 = 8$). The usefulness of the entanglement forces then increases for highly compressed systems. Note that the reduction of bond crossings remains very effective at high compression (94% for $h/h_0 = 8$).

The friction coefficient can also be deduced from the tangential and normal components of the pressure resulting from experimental measurements. Klein et al.[12] have extensively studied the compression of grafted polymer brushes under shear using SFA. However, the signal from the tangential pressure appears to be very small at low compression and is almost undetectable. Therefore, the accessible experimental values for the tangential component are not accessible for the compression ratio $h/h_0 > 0.2$. At high compression, experiments show a strong increase in the tangential component. Unfortunately, this high compression zone ($h/h_0 < 0.2$) is not accessible in DPD because of the top limit for high density. (DPD fluids are correctly described for a number density in the range of $\rho = 2$ to 9.[47]) In Figure 5, we have plotted the friction coefficient, ε, as a function of the compression ratio for both sets of simulations. The profile

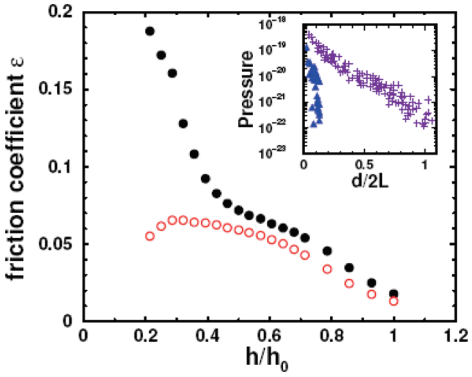

Figure 5. Friction coefficient, ε, as a function of the compression ratio. Filled and open symbols are used for entangled and nonentangled systems, respectively. The inset shows the p_{zz} (+) and p_{xz} (▲) components of the pressure tensor measured with SFA by Klein et al.[12]

$\varepsilon(z)$ is averaged to get the value of the friction, ε. The inset of this Figure shows the experimental measurements of the tangential and normal pressures taken from Klein.[14] The increase in p_{xz} is much greater than that for p_{zz} and suggests that the friction may greatly increase in the high compression zone. We observe a strong increase in the friction in the highest compression zone for entangled systems, which is in better agreement with experimental observations.

The entanglement model gives rise to a more satisfactory interpretation of the friction between the polymer brushes in DPD. The entanglement force is designed to avoid the bond crossings, and many of these crossings occur in the interpenetration zone when applying a shear rate. The entanglement contribution is then greater in the highly compressed systems, giving raise to a large increase in the friction. The model without entanglements appears to fail in this respect because of proximity of the opposite brush and the shear rate. The soft bead repulsion is insufficient to respect the topology of the polymer chains. Therefore, the entangled polymer model is of great importance in confined polymer systems using mesoscopic simulations and must be taken into account when rheological properties such as the friction are studied.

Influence of Solvent and Shear Rate. We have noted in a previous paper[39] that the addition of entanglement forces results in a swelling of the polymer brushes. The modeling at higher solvent quality has the same influence on the brush structure. In a previous work,[35] the influence of the solvent quality on the polymer brushes under shear was studied for nonentangled systems. We have performed simulations using various solvent qualities to show the influence of the entanglement potential on the general structural behavior of the brushes. Two sets of simulations have been carried: with and without the bond repulsion. Each set consists of 11 simulations with the solvent quality varying from $\Delta a_{\mathrm{pol-sol}} = -20$ to 20. The value $\Delta a_{\mathrm{pol-sol}} = a_{\mathrm{pol-sol}} - a_{\mathrm{pol-pol}}$ represents the increase/decrease in the interaction force between the polymer and solvent particles, referred to the polymer−polymer interaction taken as a reference. Therefore, a zero value refers to an athermal, Θ, solvent; negative values indicate good solvent quality, and positive values indicate poor solvent quality. The simulations are performed at a moderate compression ratio (h = 16, h/h_0 = 0.57). Each run consists of a 50 000 time step equilibration, followed by a 300 000 timestep acquisition in the canonical ensemble.

Figure 6 shows the correlation between the brush interpenetration and the friction coefficient for both sets of simulations. In the poor solvent zone, the polymer brushes

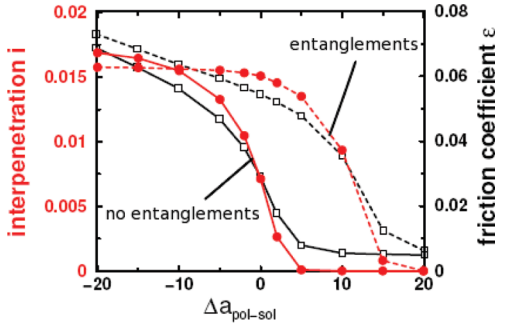

Figure 6. Interpenetration (I, circles) and friction (ε, squares) as a function of the solvent quality for entangled and nonentangled polymer brushes systems (filled and open symbols, respectively).

reject the solvent particles to form a pure solvent phase in the middle of the simulation cell. As the solvent quality increases, the brushes tend to overlap, which increases the interpenetration, I, giving rise to larger friction. The open symbols show this behavior, centered on the athermal solvent value $\Delta a_{\mathrm{pol-sol}} = 0$. For the systems with entangled polymer brushes, we observe a similar behavior, but the shrinking of the brushes occurs at poorer solvent qualities. This is in line with our previous study concerning the structure of the entangled brushes. Consequently, the position of the theta solvent may vary depending on the entanglement forces included in the polymer model.

We have seen in the previous section that the swelling of the brushes is not the only consequence of adding entanglement forces. However, the change in the friction values during the compression occurs only for strong compressions. At low compression, the friction coefficient of entangled systems remains greater than that for nonentangled systems but follows the same behavior. This can be readily explained: at low compression, the brush interpenetration stays very small, which gives a constant and small additional contribution to the friction for the entangled system.

We have conducted simulations at a low compression ratio (h = 8, h/h_0 = 0.29) to study the behavior of the entangled brushes as a function of the shear rate. As before, two sets of simulations have been performed, using values for the shear rate ranging from 0.02 to 0.2. Each run is composed of an equilibration part (50 000 timesteps) and an acquisition part (300 000 timesteps) at constant NVT. Figure 7a displays the evolution of the shear viscosity of the solvent confined to the middle of the simulation cell by the polymer brushes. A significant decrease in the viscosity is observed as the shear rate increases. This strong shear-thining effect is widely known in experimental systems and is in good agreement with recent studies using various simulation methods.[28,62−64] It can be explained by the ordering and the extension of the brushes along the shear direction (the x axis). Figure 7b shows the x-component of the chain radius of gyration as a function of the shear rate. The entangled chains appear to be stongly stretched along the shear direction, even for low shear rate values. This ordering is due to the repulsions between bonds, which force the chains to align and stretch to avoid entanglements. This constraint between the brushes results in higher values of the tangential component, p_{xz}, which results in higher viscosity.

The addition of the entanglement force shows two distinct effect that have been discussed in this section. The first consequence is to make the chains more voluminous because of this additional repulsion between the polymers. This results in the swelling of the brushes and the shift of the apparent solvent quality. This effect is not due to the

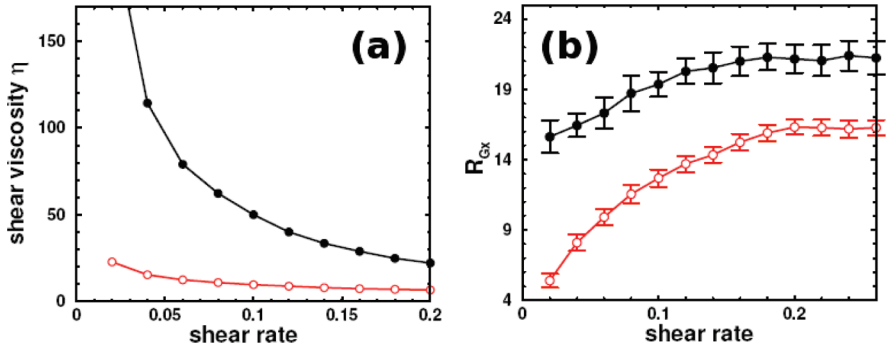

Figure 7. (a) Shear viscosity at the middle of the pore for the entangled (●) and nonentangled (○) systems as a function of the shear rate intensity. The system is at high compression ratio ($h = 8, h/h_0 = 0.29$). (b) x component of the radius of gyration as a function of the shear rate (same legend as part a).

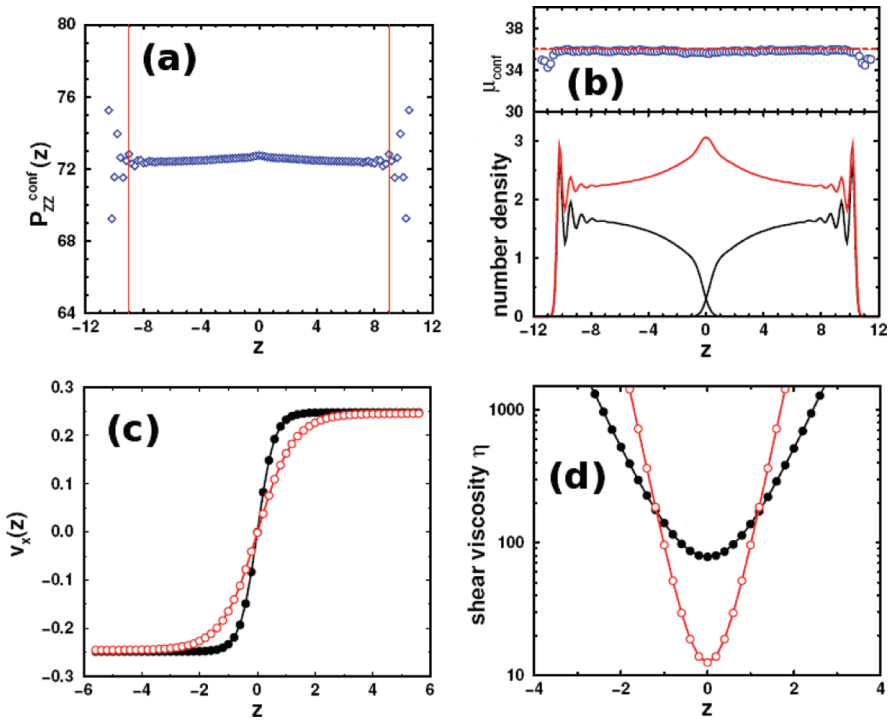

Figure 8. (a) z profile of the normal component of the pressure tensor calculated from eq 8 for an entangled system at a compression ($h/h_0 = 0.64$). (b) z profile of the configurational chemical potential calculated from eq 11 in the same system (○); the imposed chemical potential (—) and the solvent (upper curve) and brushes (lower curves) number density profiles are shown for comparison. (c) z profile of the x component of the solvent velocity for entangled (●) and nonentangled (○) systems at high compression ($h = 0.28$). The curves represent the respective sigmoidal fit. (d) Viscosity profiles corresponding to the system described in part c.

fact that the chains are entangled: the bond repulsion adds an energetical contribution to the system, which changes its structure and static properties. The second consequence of this force is that the chain topology is conserved by the removal of bond crossings. This effect becomes more visible for highly compressed chains and could not be replaced by an increase/decrease in the solvent quality. Avoiding the chain topology violations makes the chains be entangled and changes the rheological behavior of the system.

Thermodynamic Equilibrium. In this section, we detail the different analysis that must be performed for each simulation to check the thermodynamic consistency of the system. Figure 8a shows the z profile of the configurational part of the normal pressure. Except for oscillations due to the tethered particles in the surfaces, the profile is independent of z. Therefore, it allows a reliable calculation of the average components of the pressure tensor across the pore. This constant profile is only obtained by including the entanglement contribution.[39]

Figure 8b (lower part) shows the number density profiles of both the polymer brushes and the solvent particles. The system simulated here is for a high compression ratio ($h = 24$, $h/h_0 = 0.86$), which gives a small overlap zone between the brushes at the middle of the cell. The upper part shows the corresponding profile of the configurational chemical potential, μ^{conf}. Two features of this profile have to be checked for each simulation. First, the profile must be constant throughout the cell, which denotes that the chemical equilibrium is reached. Second, the chemical potential has to be close to the imposed value. The dashed line indicates the imposed value of μ^{conf}, which is in good agreement with the calculated value. There is a slight difference between the calculated and the imposed chemical potentials. Simulations under shear may cause an overheat, which is hard to dissipate: this results in a small deviation of the calculated chemical potential. (See eq 11.) This issue has been studied for various DPD thermostats.[65]

The calculation of the viscosity involves the calculation of the velocity profile of the solvent. Figure 8c displays the x

component (along the shear direction) of the solvent velocity profile for two systems with $h = 12$ with and without the entanglement forces. As the polymer chains are immersed in a good solvent, the solvent particles are carried by the brushes, which gives the characteristic shape of the velocity profile. The swelling of the polymer brushes due to the entanglement potential is visible in the solvent velocity profile, as evidenced by the strong variation of slab velocity at the middle of the cell. The profiles are fitted to a sigmoid function, which is used for a more accurate calculation of the viscosity profile.

Figure 8d shows the corresponding viscosity profiles. As mentioned before, the value used is the minimum viscosity in the middle of the pore. The influence of the entanglement model is obvious under these conditions because it dramatically increases the minimum in the profile and increases the width of the curve.

Conclusions

We have used the DPD method to perform mesoscopic simulations of polymer brushes under shear. We have included a bond repulsion force to model entangled polymer chains and compared the results with a simple nonentangled model. We have used a constant μVT algorithm to model the compression of polymer brushes under shear. The force−distance profiles are compared with scaling laws and experimental results from SFA experiments. We show that the addition of an entanglement force does not affect the scaling behavior of the polymer brushes, which is well represented in both cases. However, the use of entangled polymer chains appears to be crucial in the study of rheological properties. The value of the friction coefficient during the compression has been calculated and is in good agreement with the experimental measurement.

We have also studied the influence of the solvent quality on the structure of the polymer brushes. The chain repulsions cause a swelling of the brushes, mimicking an increase in the solvent quality. This effect is most pronounced at medium and low compression ratios. Therefore, the use of an entangled model in DPD adds an energetical contribution to the polymer−polymer interaction, which results in a shift of the chain behavior as a function of the solvent quality. We have also simulated varying shear rates for a highly compressed polymer brush system. The viscosity values show a strong shear-thining effect, as observed with other simulation methods. The model used in this work gives a better description of the polymers chains under shear and high compression.

DPD is a powerful tool for simulating the scaling behavior and the rheological properties of polymer systems far from mechanical equilibrium. The use of soft mesoscopic forces allows us to simulate large length and time scales, but the possible overlap between DPD particles may cause many topology changes in the polymer chains. This appears to be a crucial issue when simulating concentrated or confined systems. We show that the addition of entanglement forces improves the rheological properties of such systems by avoiding the polymer brush overlap. This entangled polymer system appears to be very efficient in modeling the polymer physics and rheology on the mesoscopic scale.

References and Notes

(1) Klein, J. *Annu. Rev. Mater. Sci.* **1996**, *26*, 581.
(2) Halperin, A.; Tirrell, M.; Lodge, T. P. *Adv. Polym. Sci.* **1992**, *100*, 31.
(3) Luckham, P. F. *Adv. Colloid Interface Sci.* **1991**, *34*, 191.
(4) Patel, S. S.; Tirrell, M. *Annu. Rev. Phys. Chem.* **1989**, *40*, 597.
(5) Brady, J. F.; Bossis, G. *J. Fluid Mech.* **1985**, *155*, 105.
(6) Semenov, A. N. *Langmuir* **1995**, *11*, 3560.
(7) de Gennes, P. G. *Macromolecules* **1980**, *13*, 1069.
(8) Milner, S. T. *Science* **1991**, *251*, 905.
(9) Milner, S. T.; Witten, T. A.; Cates, M. E. *Macromolecules* **1988**, *21*, 2610.
(10) de Gennes, P. G. *J. Phys. (Paris)* **1976**, *37*, 1445.
(11) Klein, J.; Kumacheva, E.; Perahia, D.; Fetters, L. J. *Acta Polym.* **1998**, *49*, 617.
(12) Taunton, H. J.; Toprakcioglu, C.; Klein, J. *Macromolecules* **1988**, *21*, 3333.
(13) Klein, J.; Kumacheva, E.; Mahalu, D.; Perahia, D.; Fetters, L. J. *Nature* **1994**, *370*, 634.
(14) Klein, J.; Perahia, D.; Warburg, S. *Nature* **1991**, *352*, 143.
(15) Klein, J. *Colloids Surf., A* **1994**, *86*, 63.
(16) Klein, J.; Kamiyama, Y.; Yoshisawa, H.; Israelachvili, J. N.; Fredrickson, G. H.; Pincus, P.; Fetters, L. J. *Macromolecules* **1993**, *26*, 5552.
(17) Murat, M.; Grest, G. S. *Phys. Rev. Lett.* **1989**, *63*, 1074.
(18) Grest, G. S. *Macromolecules* **1994**, *27*, 418.
(19) Putz, M.; Kremer, K.; Grest, G. S. *Europhys. Lett.* **2000**, *49*, 735.
(20) Kremer, K.; Grest, G. S. *J. Chem. Phys.* **1990**, *92*, 5057.
(21) Grest, G. S. *Adv. Polym. Sci.* **1999**, *138*, 149.
(22) Grest, G. S. *Curr. Opin. Colloid Interface Sci.* **1997**, *2*, 271.
(23) Doyle, P. S.; Shaqfeh, E. S. G.; Gast, A. P. *Macromolecules* **1998**, *31*, 5474.
(24) Doyle, P. S.; Shaqfeh, E. S. G.; Gast, A. P. *Phys. Rev. Lett.* **1997**, *78*, 1182.
(25) Neelov, I. M.; Borisov, O. V.; Binder, K. *Macromol. Theory Simul.* **1998**, *7*, 141.
(26) Saphiannikova, M. G.; Pryamitsyn, V. A.; Cosgrove, T. *Macromolecules* **1998**, *31*, 6662.
(27) Neelov, I. M.; Borisov, O. V.; Binder, K. *J. Non-Cryst. Solids* **1998**, 731.
(28) Kreer, T.; Muser, M. H.; Binder, K.; Klein, J. *Langmuir* **2001**, *17*, 7804.
(29) Chakrabarti, A.; Nelson, P.; Toral, R. *J. Chem. Phys.* **1994**, *100*, 748.
(30) Luettmer-Strathmann, J.; Rampf, F.; Paul, W.; Binder, K. *J. Chem. Phys.* **2008**, *128*, 064903.
(31) Masters, A. J.; Warren, P. B. *Europhys. Lett.* **1999**, *48*, 1.
(32) Hoogerbrugge, P. J.; Koelman, J. M. V. A. *Europhys. Lett.* **1992**, *19*, 155.
(33) Pal, S.; Seidel, C. *Macromol. Theory Simul.* **2006**, *15*, 668.
(34) Malfreyt, P.; Tildesley, D. J. *Langmuir* **2000**, *16*, 4732.
(35) Irfachsyad, D.; Tildesley, D. J.; Malfreyt, P. *Phys. Chem. Chem. Phys.* **2002**, *4*, 3008.
(36) Goujon, F.; Malfreyt, P.; Tildesley, D. J. *ChemPhysChem* **2004**, *5*, 457.
(37) Goujon, F.; Malfreyt, P.; Tildesley, D. J. *Mol. Phys.* **2005**, *103*, 2675.
(38) Kumar, S.; Larson, R. G. *J. Chem. Phys.* **2001**, *114*, 6937.
(39) Goujon, F.; Malfreyt, P.; Tildesley, D. J. *J. Chem. Phys.* **2008**, *129*, 034902.
(40) Kong, Y.; Manke, C. W.; Madden, W. G.; Schlijper, A. G. *Int. J. Thermophys.* **1994**, *15*, 1093.
(41) Schlijper, A. G.; Hoogerbrugge, P. J.; Manke, C. W. *J. Rheol.* **1995**, *39*, 567.
(42) Muller-Plathe, F. *ChemPhysChem* **2002**, *3*, 754.
(43) Baschnagel, J.; Binder, K.; Doruker, P.; Gusev, A. A.; Hahn, O.; Kremer, K.; Mattice, W. L.; Muller-Plathe, F.; Murat, M.; Paul, W.; Santos, S.; Suter, U. W.; Tries, V. *Adv. Polym. Sci.* **2000**, *152*, 41.
(44) Padding, J. T.; Briels, W. J. *J. Chem. Phys.* **2002**, *117*, 925.
(45) Forrest, B. M.; Suter, U. W. *J. Chem. Phys.* **1995**, *102*, 7256.
(46) Chang, R.; Ayton, G. S.; Voth, G. A. *J. Chem. Phys.* **2005**, *122*, 244716.
(47) Groot, R. D.; Warren, P. B. *J. Chem. Phys.* **1997**, *107*, 4423.
(48) Irving, J. H.; Kirkwood, J. G. *J. Chem. Phys.* **1950**, *18*, 817.
(49) Walton, J. P. R. B.; Tildesley, D. J.; Rowlinson, J. S.; Henderson, J. R. *Mol. Phys.* **1983**, *48*, 1357.
(50) Barnes, H. A.; Hutton, J. F.; Walters, K. *An Introduction to Rheology*; Elsevier: Amsterdam, 1989.
(51) Widom, B. *J. Chem. Phys.* **1963**, *39*, 2808.
(52) Widom, B. *J. Stat. Phys.* **1978**, *19*, 563.
(53) Powles, J. G.; Baker, S. E.; Evans, W. A. B. *J. Chem. Phys.* **1994**, *101*, 4098.
(54) Powles, J. G.; Evans, W. A. B.; Quirke, N. *Mol. Phys.* **1982**, *46*, 1347.
(55) Powles, J. G.; Holtz, B.; Evans, W. A. B. *J. Chem. Phys.* **1994**, *101*, 7804.

(56) Allen, M. P.; Tildesley, D. J. *Computer Simulation of Liquids*; Clarendon: Oxford, U.K., 1987.
(57) Frenkel, D.; Smit, B. *Understanding Molecular Simulation: From Algorithms to Applications*; Academic Press: London, 1996.
(58) Yao, J.; Greenkorn, R. A.; ChaoYao, K. C. *Mol. Phys.* **1982**, *46*, 587.
(59) Alexander, S. *J. Phys. (Paris)* **1977**, *38*, 983.
(60) de Gennes, P. G. *Adv. Colloid Interface Sci.* **1987**, *27*, 189.
(61) Taunton, H. J.; Toprakcioglu, C.; Fetters, L. J.; Klein, J. *Macromolecules* **1990**, *23*, 571.
(62) Varnik, F.; Binder, K. *J. Chem. Phys.* **2002**, *117*, 6336.
(63) Kreer, T.; Muser, M. H.; Binder, K. *Comput. Phys. Commun.* **2002**, *147*, 358.
(64) Peters, G. H.; Tildesley, D. J. *Phys. Rev. E* **1995**, *52*, 1882.
(65) Pastorino, C.; Kreer, T.; Muller, M; Binder, K. *Phys. Rev. E* **2007**, *76*, 026706.